ACS chemical biology

pubs.acs.org/acschemicalbiology

Letter

Bioorthogonal Cyclopropenones for Investigating RNA Structure

Sharon Chen,[‖] Christopher D. Sibley,[‖] Brandon Latifi, Sumirtha Balaratnam, Robert S. Dorn, Andrej Lupták, John S. Schneekloth, Jr.,* and Jennifer A. Prescher*

Cite This: *ACS Chem. Biol.* 2024, 19, 2406−2411

Read Online

ACCESS | Metrics & More | Article Recommendations | Supporting Information

ABSTRACT: RNA sequences encode structures that impact protein production and other cellular processes. Misfolded RNAs can also potentiate disease, but a complete picture is lacking. To establish more comprehensive and accurate RNA structure−function relationships, new methods are needed to interrogate RNA in native environments. Existing tools rely primarily on electrophiles that are constitutively "on" or triggered by UV light, often resulting in high background. Here we describe an alternative, chemically triggered approach to cross-link RNAs using bioorthogonal cyclopropenones (CpOs). These reagents selectively react with phosphines to provide ketenes—electrophiles that can trap neighboring nucleophiles to forge covalent cross-links. As a proof-of-concept, we conjugated a CpO motif to thiazole orange (TO-1). TO-1−CpO bound selectively to a model RNA aptamer (Mango) with nanomolar affinity, as confirmed by fluorescence turn-on. After phosphine administration, covalent cross-links were formed between the CpO and RNA. Cross-linking was both time and dose dependent. We further applied the chemically triggered tools to model RNAs under biologically relevant conditions. Collectively, this work expands the toolkit of probes for studying RNA and its native conformations.

INTRODUCTION

RNA is best known for its role as an information carrier in protein synthesis.[1] However, only 2% of known RNAs are translated. The remaining 98% comprise noncoding RNAs (ncRNAs) that play key roles in cellular processes.[2,3] These functions are dependent on the RNA structure, which is not static. RNA can adopt a variety of conformations in response to various stimuli,[4−6] and each can regulate a distinct biological process. For example, the G-quadruplex GQ-2 in the Bcl-x pre-mRNA regulates apoptosis. GQ-2 is highly structured, and its stabilization can trigger splicing, resulting in cell death.[7] Although the role of GQ-2 has been elucidated, the structure−function relationships of most RNAs remain largely unknown.

Teasing apart the subtle dynamic changes associated with RNAs (and their downstream effects) requires methods to examine RNA structural heterogeneity in physiological environments.[8−10] Since sequence information alone cannot be used to accurately predict dynamics, methods to examine the scope of structural variability are needed. Classic biophysical approaches (e.g., X-ray crystallography[11−13] and NMR[14−16]) offer high resolution, but place limitations on RNA size and environment. Chemical probing methods, by contrast, can tag RNAs of all lengths in live cells.[17−19] These reagents selectively label solvent accessible nucleobases[20−22] or 2′-hydroxyl groups, and when combined with next generation sequencing, they can be used to predict base-pairing interactions associated with RNA secondary structure.[23−26] However, most chemical probes are "always on" and cannot easily be used to investigate RNAs in response to discrete stimuli. They are thus limited in their ability to report on conformational dynamics. Photoactivatable versions have been developed to address this issue but cannot be easily translated to more heterogeneous environments owing to their need for UV irradiation.[27]

To address the need for more biofriendly RNA probes, we aimed to develop bioorthogonal chemistries for examining RNA structures. Many bioorthogonal reagents are compact, imparting minimal-to-no perturbation. In addition, bioorthogonal groups can react on demand and label the desired targets. One handle of particular interest to our groups is cyclopropenone (CpO). CpO motifs are small functional groups that react with biocompatible phosphines to generate electrophilic ketene−ylide intermediates (Figure 1). These intermediates can be trapped with exogenous probes in a classic bioorthogonal sense. The ketenes can also be trapped by neighboring nucleophiles (e.g., hydroxyl groups and nucleobases), leading to cross-linked products. In this latter case, if the CpO is localized to a defined RNA, then we could potentially probe conformational changes within that vicinity. Ketene formation could also be initiated at any time, enabling RNA structural changes to be examined in response to various stimuli.

Received: September 18, 2024
Revised: November 6, 2024
Accepted: November 25, 2024
Published: December 6, 2024

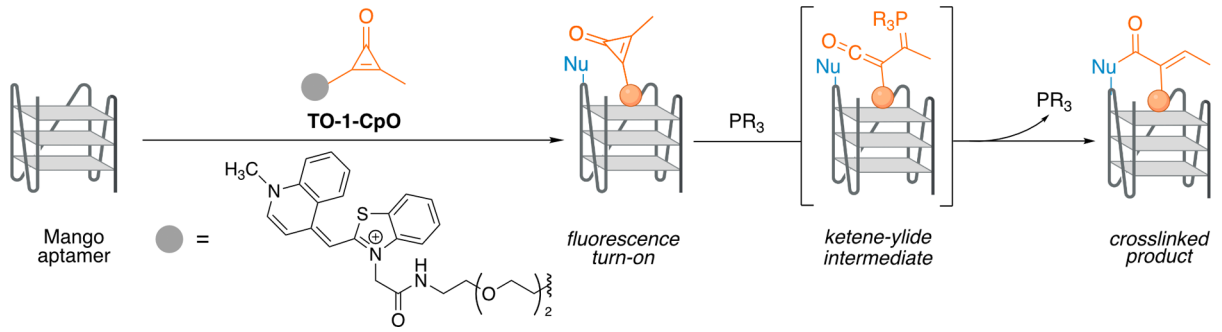

Figure 1. Cyclopropenones as chemically triggered probes for examining RNA structure. In this work, the Mango aptamer was used as a model to demonstrate CpO-mediated cross-linking.

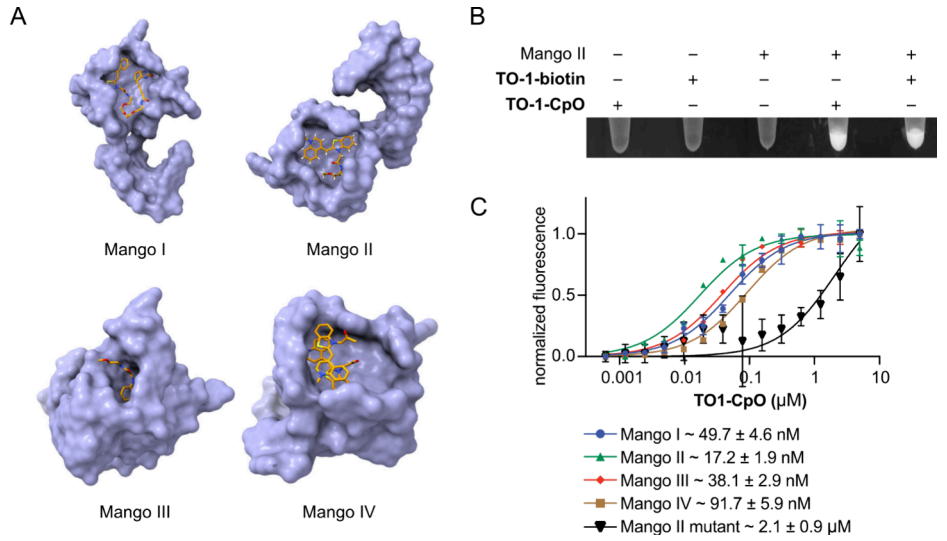

Figure 2. TO-1−CpO binds Mango II with nanomolar affinity. (A) Crystal structures of each Mango aptamer with TO-1−biotin depicted as space filling models. Mango I (PDB: 5V3F), Mango II (PDB: 6C63), Mango III (PDB: 6E8S), Mango IV (PDB: 6V9D). (B) Fluorescence turn-on analyses of Mango II samples incubated with TO-1−biotin, TO-1−CpO, or no reagent. (C) Fluorescence measurements resulting from TO-1−CpO (0−10 μM) incubated with each Mango aptamer. These data were used to calculate binding affinity (K_D) of TO-1−CpO for each flavor of Mango, reported below the graph. Error bars represent the standard error of the mean for n = 3 experiments.

Here, we report a platform for sampling RNA structures using bioorthogonal CpO motifs. We previously applied the CpO−phosphine reaction to both label and cross-link proteins.[28,29] In this work, we show that the transformation can be similarly used to study RNA conformations. The reaction was evaluated with model nucleophiles for trapping structured RNA motifs. Cross-linking was further examined with a model aptamer−ligand pair. Collectively, this work establishes a new chemical method for examining RNA structure using a conditionally activated chemical probe.

RESULTS AND DISCUSSION

Design, Synthesis, And Characterization of TO-1−CpO. To develop a bioorthogonal platform for triggered cross-linking, we initially focused on the fluorogenic RNA aptamer Mango (Figure 1). Mango is a laboratory-evolved, highly structured RNA that forms a three-tiered G-quadruplex motif and binds the fluorogenic dye thiazole orange biotin (TO-1−biotin) with low nanomolar affinity.[30] This ligand is synthetically accessible and exhibits enhanced fluorescence turn-on upon binding to Mango.[31−33] We prepared a TO-1 variant comprising a bioorthogonal CpO motif (TO-1−CpO, Scheme S1), and examined whether the probe could be activated by bioorthogonal phosphines. Phosphine treatment was expected to initiate a cross-link between the ligand and the aptamer only in the presence of nearby nucleophiles. The absence of a suitable trap would instead yield an innocuous quenched product (Figure S1A). We also surmised that ribose hydroxyl groups could serve as nucleophiles, based on earlier work demonstrating that tyrosine phenol groups could forge cross-links with CpO-modified proteins.[28] TO-1−CpO was incubated with aniline and benzylamine (to simulate nucleotide trapping) in the presence of PTA, a commercially available and water-soluble phosphine.[34] Cross-linked products were observed in the presence of either amine trap (Figures S1 and S2), confirming that nucleophiles present on nucleotides could react with activated CpO motifs.

Investigating the Binding and Cross-Linking between TO-1−CpO and Mango. We next pursued CpO-mediated cross-linking with the Mango aptamer as a model RNA. Given the four distinct variants of Mango available,[35−38] we initially examined the ligand-bound crystal structures (Figure 2A). The native biotin fragment was used to approximate the location of CpO. The models suggested that the CpO unit would remain solvent exposed in Mango II, and thus be accessible to the phosphine trigger. We therefore moved forward with this aptamer. TO-1−CpO was incubated with Mango II, and fluorescence measurements were used to

https://doi.org/10.1021/acschembio.4c00633
ACS Chem. Biol. 2024, 19, 2406−2411

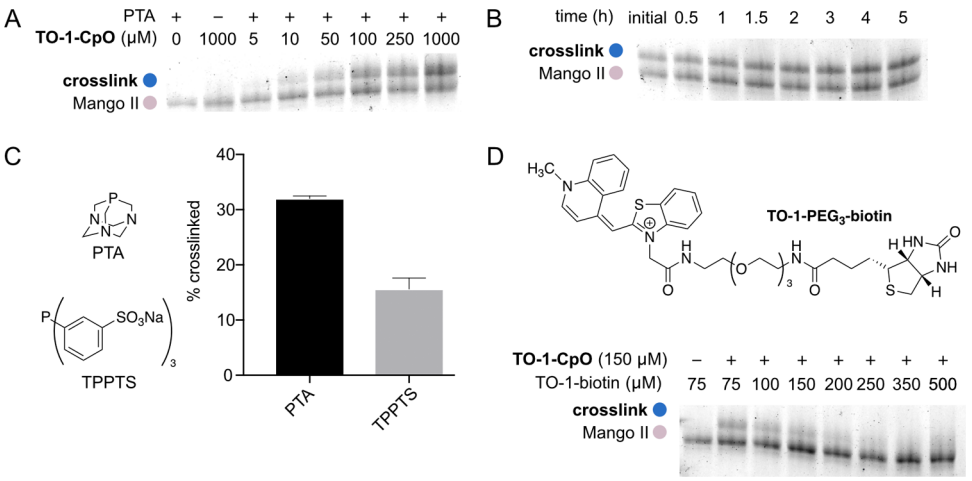

Figure 3. CpO-mediated cross-linking of Mango II is dependent on ligand concentration, time, and phosphine nucleophilicity. (A) Denaturing PAGE analysis of cross-linking reactions. 5′-Cy5 labeled Mango II (10 μM) was incubated with varying concentrations of TO-1−CpO and PTA (10 mM). (B) Denaturing PAGE analysis of cross-linking time dependence. 5′-Cy5 labeled Mango II (10 μM) was incubated with TO-1−CpO (250 μM) and PTA (10 mM), and samples were analyzed over 5 h. (C) Quantification of relative cross-linking yields with various phosphine triggers. 5′-Cy5 labeled Mango II (10 μM) was incubated for 2 h with various phosphines (10 mM), and reaction products were analyzed via denaturing PAGE. Error bars represent the standard error of the mean for independent replicate experiments (n = 4 for PTA and n = 3 for TPTPS). (D) Denaturing PAGE analysis of cross-linking experiments performed in the presence of competing ligand (TO-1−biotin). TO-1−biotin (75−500 μM) was added to reactions comprising Mango II (10 μM), TO-1−CpO (150 μM), and PTA (10 mM).

confirm ligand binding. As expected, signal turn-on was comparable to that observed with the known ligand TO-1−biotin (Figure 2B). The binding affinities (K_D) for the remaining Mango aptamers were also determined. TO-1−CpO exhibited the tightest binding with Mango II. Importantly, binding was dramatically reduced with an inactive Mango II mutant, where the guanines involved in G-quadruplex formation were mutated to cytidines (Figure 2C).

Once ligand binding was confirmed, we aimed to cross-link TO-1−CpO to the Mango II aptamer and examine the effect of TO-1−CpO concentration on cross-linking efficiency. 5′-Cy5-labeled Mango II was incubated with varying amounts of TO-1−CpO (0−1000 μM), and the cross-linking reactions were assessed with denaturing PAGE. Gels were scanned using differential filters to visualize both the unmodified and cross-linked RNAs. Cross-linking was first observed with 10 μM ligand, and the fluorescence intensity of the band under the TO filter increased with larger amounts of ligand present (Figure 3A). All subsequent experiments were performed with excess ligand to maximize cross-linking yield.

Optimizing CpO-Mediated Cross-Linking Conditions. We further evaluated the time and temperature dependence of the reaction to maximize cross-linking yields. Cross-linking increased over 2 h prior to reaching a plateau (Figure 3B). Increased labeling was also observed at higher temperatures (Figure S4). Although cross-linking yields at 25 and 37 °C were similar, 37 °C was chosen for subsequent experiments to mimic physiological conditions.

We next examined the effect of phosphine nucleophilicity on relative cross-linking yield. More reactive phosphines enable rapid cross-linking, but these same reagents are more susceptible to oxidation.[28] Ten phosphines were examined using the optimized parameters (Table S1). Included in this group were well-known phosphine ligands (TPP, CyDPP, PTA, and PTABS) and biological reagents (THMP, THPP, and TCEP). Cross-linking was evaluated using denaturing PAGE, and relative efficiencies were calculated by gel densitometry. Differential cross-linking was observed, and the best performing phosphines generally included the most nucleophilic reagents (TPP, CyDPP, PTA, THMP). We did not move forward with TPP, CyDPP, or THMP though, given their poor solubility in aqueous buffers. In addition, the negatively charged phosphine reagents (TPPTS and CyDPPDS) resulted in less cross-linking compared to their neutral counterparts. We attributed this result to charge repulsion with the phosphate backbone of RNA. Based on the remaining phosphines that exhibited good labeling yields, PTA was chosen over PTABS to minimize charge repulsion effects (Figure 3C).

Examining the Specificity of CpO-Mediated Cross-Linking. We further investigated whether TO-1−CpO binding to the target RNA was necessary, or if cross-linking was ubiquitous regardless of the aptamer present. In one experiment, we included Mango's cognate ligand, TO-1−biotin, as a competitor. Reactions were performed with TO-1−CpO held at a constant concentration (150 μM) and with varying TO-1−biotin (75−500 μM). Cross-linking decreased as concentration of TO-1−biotin increased, suggesting that both ligands occupy the same binding site (Figure 3D). We also examined additional probes lacking key elements for cross-linking, TO-1−NH_2 and Ph−CpO. TO-1−NH_2 contains the dye and can bind to the Mango II aptamer but lacks the CpO, whereas Ph−CpO cannot localize to the aptamer but contains the CpO. Importantly, when these negative control probes were used in place of TO-1−CpO, cross-linking was not observed. These observations confirm that each element of TO-1−CpO plays an essential role in cross-linking to the RNA (Figure S5A).

The specificity of the reaction was further examined using other structured nucleic acids. The panel included a range of motifs [e.g., hTERT (an RNA pseudoknot), cMyc IRES (an RNA hairpin), or RNase P (a complex RNA)) not known to interact with TO-1. As expected, minimal to no-cross-linking was observed with nontarget RNAs (Figure S5B,C). Specificity for Mango II was further showcased when TO-1−CpO was incubated with an inactive variant of the Mango II aptamer,

https://doi.org/10.1021/acschembio.4c00633
ACS Chem. Biol. 2024, 19, 2406−2411

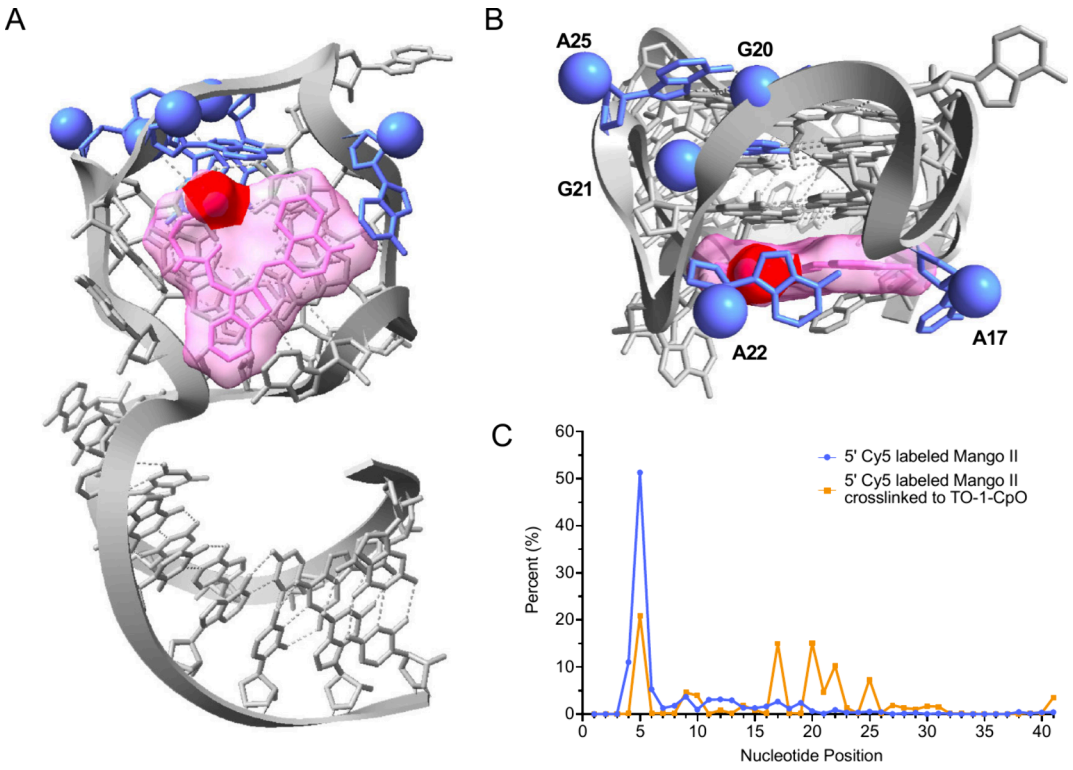

Figure 4. Proximity-dependent cross-linking was observed with TO-1−CpO and Mango II. (A) Crystal structure of Mango II aptamer docked with truncated TO-1−biotin. Approximate position of the CpO motif is highlighted in red. Sites of reactivity are colored in blue. (B) Close up of the binding domain highlighting the five modified bases. (C) Sequencing analyses of reverse transcribed Mango II aptamer. RT stops observed with TO-1−CpO modified Mango II aptamer (blue) were significantly higher at five sites in comparison to the unmodified RNA (orange).

where key guanines involved in forming the G-quadruplex were mutated to cytidines (Figure S6). Minimal cross-linking was observed at ligand concentrations below 100 μM. Some covalent trapping was observed at higher concentrations, but the efficiency was much lower than that observed with wild-type Mango II.

TO-1−CpO was further incubated with other Mango aptamers in the presence of phosphine. Cross-linked product formation was analyzed by denaturing PAGE and MALDI-MS (Figure S7). The most labeling was achieved with Mango II, confirming our hypothesis regarding accessibility (Figure S8). Cross-linking with other Mango aptamers was also observed, but to a lesser extent. Collectively, these results demonstrate that CpO-mediated cross-linking between TO-1−CpO and Mango is specific to both the RNA sequence and three-dimensional structure.

Identifying the Proximity Dependence and Location of the Cross-Link. To gain insight into the specificity of cross-linking, we incubated 5′ Cy5 labeled Mango II, 3′ Cy5 labeled Mango II, and TO-1−CpO cross-linked Mango II with RNase T1. This nuclease cleaves specifically after guanines, which are abundant in the Mango aptamer. The resulting cleavage patterns were evaluated using denaturing PAGE (Figure S9). A laddering effect was observed with the 5′ Cy5 labeled Mango II and 3′ Cy5 labeled Mango II samples. The same pattern was not observed with TO-1−CpO cross-linked aptamer, suggesting that the probe does not nonspecifically label the termini.

To identify specific sites of cross-linking, 5′ Cy5 labeled Mango II and the TO-1−CpO cross-linked variant were reverse transcribed. MMLV reverse transcriptase was chosen because of its high sensitivity to RNA modifications. In our case, the TO-1 moiety was likely large enough to terminate reverse transcription at the sites of labeling and thus reveal the positions of interest. Reverse-transcribed samples were amplified and submitted for high-throughput sequencing. Terminations at positions 17, 20, 21, 22, and 25 were significantly higher with the TO-1−CpO cross-linked Mango II when compared to the (un-cross-linked) 5′ Cy5 labeled Mango II (Figure 4). When these sites were mapped onto the crystal structure, the proximity dependence of the cross-linking was immediately apparent (Figure 4A,B). Labeled nucleotides (blue) are localized near the putative CpO position (dark pink) in the top half of the aptamer. Termination was not observed on other parts of the aptamer, demonstrating that the reaction is specific and dependent on TO-1−CpO recognizing the binding site on Mango II.

CONCLUSIONS

Structure plays a critical role in RNA function, and elucidating how specific conformations influence molecular recognition is important to understanding biological processes. Great progress has been made in deciphering RNA structure−function relationships using SHAPE and other tools.[24,39−41] However, most reagents lack temporal control, making it difficult to study dynamic changes. Photoactivatable versions have been developed to address this issue, but the necessary irradiation is potentially harmful to nucleic acids. The community would benefit from biocompatible and conditional ("triggerable") probes to study the RNA dynamics.

Here, we showcased CpO motifs for interrogating RNA by covalently modifying RNAs near ligand binding sites. CpOs were chemically activated by phosphines to tag three-

https://doi.org/10.1021/acschembio.4c00633
ACS Chem. Biol. 2024, 19, 2406−2411

dimensional RNA structures. Triggered cross-linking was achieved using the Mango II aptamer as a model system. We further demonstrated that the reaction is dependent on the ligand concentration, time, temperature, and phosphine nucleophilicity. In addition, we determined that the labeling is probe specific and proximity dependent. Finally, sequencing revealed the positions where covalent linkages were forged. Importantly, sites of modification were proximal to the known ligand binding site, indicating that molecular recognition of the probe is important for labeling nucleotides that are distal in sequence but proximal in a three-dimensional structure.

Future directions will focus on expanding the scope and efficiency of CpO-mediated cross-linking. Applications in cells and other physiologically relevant environments are envisioned. Appropriately modified reagents could be used to examine RNA conformational dynamics in response to stress, protein/ligand binding, and other stimuli. Additionally, the bioorthogonal cross-linking strategy could be used to identify biomolecules interacting with RNAs of interest, to covalently tag RNAs, or to map binding sites of ligands to complex RNAs. In this case, designer ligands with longer linkers could bridge (and potentially trap) neighboring proteins. Such experiments will continue to expand our understanding of RNA structure−function relationships and the molecular recognition of RNA in biological settings.

■ ASSOCIATED CONTENT

Supporting Information

The Supporting Information is available free of charge at https://pubs.acs.org/doi/10.1021/acschembio.4c00633.

General materials and methods, Figures S1−S9, Table S1, synthetic procedures, and small molecule/conjugate characterization data (PDF)

■ AUTHOR INFORMATION

Corresponding Authors

John S. Schneekloth, Jr. − *Chemical Biology Laboratory, National Cancer Institute, Frederick, Maryland 21702, United States*; Email: jay.schneekloth@nih.gov

Jennifer A. Prescher − *Department of Chemistry, Department of Molecular Biology & Biochemistry, and Department of Pharmaceutical Sciences, University of California, Irvine, California 92697, United States*; orcid.org/0000-0002-9250-4702; Email: jpresche@uci.edu

Authors

Sharon Chen − *Department of Chemistry, University of California, Irvine, California 92697, United States*

Christopher D. Sibley − *Chemical Biology Laboratory, National Cancer Institute, Frederick, Maryland 21702, United States*

Brandon Latifi − *Department of Pharmaceutical Sciences, University of California, Irvine, California 92697, United States*

Sumirtha Balaratnam − *Chemical Biology Laboratory, National Cancer Institute, Frederick, Maryland 21702, United States*

Robert S. Dorn − *Department of Chemistry, University of California, Irvine, California 92697, United States*; orcid.org/0000-0001-7683-2151

Andrej Lupták − *Department of Chemistry, Department of Molecular Biology & Biochemistry, and Department of Pharmaceutical Sciences, University of California, Irvine, California 92697, United States*; orcid.org/0000-0002-0632-5442

Complete contact information is available at: https://pubs.acs.org/10.1021/acschembio.4c00633

Author Contributions

‖S.C. and C.D.S. made equal contributions.

Notes

The authors declare no competing financial interest.

■ ACKNOWLEDGMENTS

This work was supported by the U.S. National Institutes of Health (R01 GM 1262226 to J.A.P.), the Chan-Zuckerberg Initiative (J.A.P.) and Intramural Program of the NIH, NCI, Center for Cancer Research (J.S.S.). We thank Benjamin Katz and Felix Grün at the UC Irvine Mass Spectrometry facility and the NCI Biophysics Resources center for assistance with mass spectrometry. We also thank members of the Prescher, Lupták, and Schneekloth labs for insightful discussions. BioRender (https://biorender.com/) was used to prepare some figures in this text.

■ REFERENCES

(1) Alberts, B.; Johnson, A.; Lewis, J.; Raff, M.; Roberts, K.; Walter, P. From RNA to Protein. In *Molecular Biology of the Cell*, 4th ed.; Garland Science, 2002.

(2) Meyer, S. M.; Williams, C. C.; Akahori, Y.; Tanaka, T.; Aikawa, H.; Tong, Y.; Childs-Disney, J. L.; Disney, M. D. Small Molecule Recognition of Disease-Relevant RNA Structures. *Chem. Soc. Rev.* **2020**, *49* (19), 7167−7199.

(3) Sharp, P. A. The Centrality of RNA. *Cell* **2009**, *136* (4), 577−580.

(4) Ganser, L. R.; Kelly, M. L.; Herschlag, D.; Al-Hashimi, H. M. The Roles of Structural Dynamics in the Cellular Functions of RNAs. *Nat. Rev. Mol. Cell Biol.* **2019**, *20* (8), 474−489.

(5) Mustoe, A. M.; Brooks, C. L.; Al-Hashimi, H. M. Hierarchy of RNA Functional Dynamics. *Annu. Rev. Biochem.* **2014**, *83*, 441−466.

(6) Spitale, R. C.; Incarnato, D. Probing the Dynamic RNA Structurome and Its Functions. *Nat. Rev. Genet.* **2023**, *24* (3), 178−196.

(7) Le Sénéchal, R.; Keruzoré, M.; Quillévéré, A.; Loaëc, N.; Dinh, V.-T.; Reznichenko, O.; Guixens-Gallardo, P.; Corcos, L.; Teulade-Fichou, M.-P.; Granzhan, A.; Blondel, M. Alternative Splicing of *BCL-x* Is Controlled by RBM25 Binding to a G-Quadruplex in *BCL-x* Pre-mRNA. *Nucleic Acids Res.* **2023**, *51* (20), 11239−11257.

(8) Zhang, Y.; Yang, M.; Duncan, S.; Yang, X.; Abdelhamid, M. A. S.; Huang, L.; Zhang, H.; Benfey, P. N.; Waller, Z. A. E.; Ding, Y. G-Quadruplex Structures Trigger RNA Phase Separation. *Nucleic Acids Res.* **2019**, *47* (22), 11746−11754.

(9) Yang, X.; Yu, H.; Duncan, S.; Zhang, Y.; Cheema, J.; Liu, H.; Benjamin Miller, J.; Zhang, J.; Kwok, C. K.; Zhang, H.; Ding, Y. RNA G-Quadruplex Structure Contributes to Cold Adaptation in Plants. *Nat. Commun.* **2022**, *13* (1), 6224.

(10) Cao, X.; Zhang, Y.; Ding, Y.; Wan, Y. Identification of RNA Structures and Their Roles in RNA Functions. *Nat. Rev. Mol. Cell Biol.* **2024**, *25*, 784.

(11) Doudna, J. A.; Cate, J. H. RNA Structures Determined by X-Ray Crystallography. In *RNA*; Söll, D., Nishimura, S., Moore, P., Eds.; Pergamon: Oxford, 2001; Chapter 3, pp 49−60. DOI: DOI: 10.1016/B978-008043408-7/50024-1.

(12) Edwards, A. L.; Garst, A. D.; Batey, R. T. Determining Structures of RNA Aptamers and Riboswitches by X-Ray Crystallography. *Methods Mol. Biol. Clifton NJ.* **2009**, *535*, 135−163.

(13) Jackson, R. W.; Smathers, C. M.; Robart, A. R. General Strategies for RNA X-Ray Crystallography. *Molecules* **2023**, *28* (5), 2111.
(14) Fürtig, B.; Richter, C.; Wöhnert, J.; Schwalbe, H. NMR Spectroscopy of RNA. *ChemBioChem.* **2003**, *4* (10), 936−962.
(15) Latham, M. P.; Brown, D. J.; McCallum, S. A.; Pardi, A. NMR Methods for Studying the Structure and Dynamics of RNA. *ChemBioChem.* **2005**, *6* (9), 1492−1505.
(16) Varani, G.; Aboul-ela, F.; Allain, F. H.-T. NMR Investigation of RNA Structure. *Prog. Nucl. Magn. Reson. Spectrosc.* **1996**, *29* (1), 51−127.
(17) Wang, X.-W.; Liu, C.-X.; Chen, L.-L.; Zhang, Q. C. RNA Structure Probing Uncovers RNA Structure-Dependent Biological Functions. *Nat. Chem. Biol.* **2021**, *17* (7), 755−766.
(18) Mitchell, D.; Assmann, S. M.; Bevilacqua, P. C. Probing RNA Structure in Vivo. *Curr. Opin. Struct. Biol.* **2019**, *59*, 151−158.
(19) Ziehler, W. A.; Engelke, D. R. Probing RNA Structure with Chemical Reagents and Enzymes. *Curr. Protoc. Nucleic Acid Chem.* **2000**, *00*, 6.1.1−6.1.21.
(20) Wang, P. Y.; Sexton, A. N.; Culligan, W. J.; Simon, M. D. Carbodiimide Reagents for the Chemical Probing of RNA Structure in Cells. *RNA* **2019**, *25* (1), 135−146.
(21) Noller, H. F.; Chaires, J. B. Functional Modification of 16S Ribosomal RNA by Kethoxal. *Proc. Natl. Acad. Sci. U. S. A.* **1972**, *69* (11), 3115−3118.
(22) Peattie, D. A.; Gilbert, W. Chemical Probes for Higher-Order Structure in RNA. *Proc. Natl. Acad. Sci. U. S. A.* **1980**, *77* (8), 4679−4682.
(23) Deigan, K. E.; Li, T. W.; Mathews, D. H.; Weeks, K. M. Accurate SHAPE-Directed RNA Structure Determination. *Proc. Natl. Acad. Sci. U. S. A.* **2009**, *106* (1), 97−102.
(24) Spitale, R. C.; Crisalli, P.; Flynn, R. A.; Torre, E. A.; Kool, E. T.; Chang, H. Y. RNA SHAPE Analysis in Living Cells. *Nat. Chem. Biol.* **2013**, *9* (1), 18−20.
(25) Spitale, R. C.; Flynn, R. A.; Torre, E. A.; Kool, E. T.; Chang, H. Y. RNA Structural Analysis by Evolving SHAPE Chemistry. *WIREs RNA* **2014**, *5* (6), 867−881.
(26) Weeks, K. M.; Mauger, D. M. Exploring RNA Structural Codes with SHAPE Chemistry. *Acc. Chem. Res.* **2011**, *44* (12), 1280−1291.
(27) Feng, C.; Chan, D.; Joseph, J.; Muuronen, M.; Coldren, W. H.; Dai, N.; Corrêa, I. R.; Furche, F.; Hadad, C. M.; Spitale, R. C. Light-Activated Chemical Probing of Nucleobase Solvent Accessibility inside Cells. *Nat. Chem. Biol.* **2018**, *14* (3), 276−283.
(28) Row, R. D.; Nguyen, S. S.; Ferreira, A. J.; Prescher, J. A. Chemically Triggered Crosslinking with Bioorthogonal Cyclopropenones. *Chem. Commun.* **2020**, *56* (74), 10883−10886.
(29) Row, R. D.; Shih, H.-W.; Alexander, A. T.; Mehl, R. A.; Prescher, J. A. Cyclopropenones for Metabolic Targeting and Sequential Bioorthogonal Labeling. *J. Am. Chem. Soc.* **2017**, *139* (21), 7370−7375.
(30) Dolgosheina, E. V.; Jeng, S. C. Y.; Panchapakesan, S. S. S.; Cojocaru, R.; Chen, P. S. K.; Wilson, P. D.; Hawkins, N.; Wiggins, P. A.; Unrau, P. J. RNA Mango Aptamer-Fluorophore: A Bright, High-Affinity Complex for RNA Labeling and Tracking. *ACS Chem. Biol.* **2014**, *9* (10), 2412−2420.
(31) Autour, A.; Jeng, S. C. Y.; Cawte, A. D.; Abdolahzadeh, A.; Galli, A.; Panchapakesan, S. S. S.; Rueda, D.; Ryckelynck, M.; Unrau, P. J. Fluorogenic RNA Mango Aptamers for Imaging Small Non-Coding RNAs in Mammalian Cells. *Nat. Commun.* **2018**, *9* (1), 656.
(32) Cawte, A. D.; Unrau, P. J.; Rueda, D. S. Live Cell Imaging of Single RNA Molecules with Fluorogenic Mango II Arrays. *Nat. Commun.* **2020**, *11* (1), 1283.
(33) Jeng, S. C. Y.; Chan, H. H. Y.; Booy, E. P.; McKenna, S. A.; Unrau, P. J. Fluorophore Ligand Binding and Complex Stabilization of the RNA Mango and RNA Spinach Aptamers. *RNA* **2016**, *22* (12), 1884−1892.
(34) Heiss, T. K.; Dorn, R. S.; Ferreira, A. J.; Love, A. C.; Prescher, J. A. Fluorogenic Cyclopropenones for Multicomponent, Real-Time Imaging. *J. Am. Chem. Soc.* **2022**, *144* (17), 7871−7880.
(35) Trachman, R. J.; Demeshkina, N. A.; Lau, M. W. L.; Panchapakesan, S. S. S.; Jeng, S. C. Y.; Unrau, P. J.; Ferré-D'Amaré, A. R. Structural Basis for High-Affinity Fluorophore Binding and Activation by RNA Mango. *Nat. Chem. Biol.* **2017**, *13* (7), 807−813.
(36) Trachman, R. J.; Autour, A.; Jeng, S. C. Y.; Abdolahzadeh, A.; Andreoni, A.; Cojocaru, R.; Garipov, R.; Dolgosheina, E. V.; Knutson, J. R.; Ryckelynck, M.; Unrau, P. J.; Ferré-D'Amaré, A. R. Structure and Functional Reselection of the Mango-III Fluorogenic RNA Aptamer. *Nat. Chem. Biol.* **2019**, *15* (5), 472−479.
(37) Trachman, R. J. I.; Abdolahzadeh, A.; Andreoni, A.; Cojocaru, R.; Knutson, J. R.; Ryckelynck, M.; Unrau, P. J.; Ferré-D'Amaré, A. R. Crystal Structures of the Mango-II RNA Aptamer Reveal Heterogeneous Fluorophore Binding and Guide Engineering of Variants with Improved Selectivity and Brightness. *Biochemistry* **2018**, *57* (26), 3544−3548.
(38) Trachman, R. J.; Autour, A.; Jeng, S. C. Y.; Abdolahzadeh, A.; Andreoni, A.; Cojocaru, R.; Garipov, R.; Dolgosheina, E. V.; Knutson, J. R.; Ryckelynck, M.; Unrau, P. J.; Ferré-D'Amaré, A. R. Structure and Functional Reselection of the Mango-III Fluorogenic RNA Aptamer. *Nat. Chem. Biol.* **2019**, *15* (5), 472−479.
(39) Spitale, R. C.; Incarnato, D. Probing the Dynamic RNA Structurome and Its Functions. *Nat. Rev. Genet.* **2023**, *24* (3), 178−196.
(40) Siegfried, N. A.; Busan, S.; Rice, G. M.; Nelson, J. A. E.; Weeks, K. M. RNA Motif Discovery by SHAPE and Mutational Profiling (SHAPE-MaP). *Nat. Methods* **2014**, *11* (9), 959−965.
(41) Wang, X.-W.; Liu, C.-X.; Chen, L.-L.; Zhang, Q. C. RNA Structure Probing Uncovers RNA Structure-Dependent Biological Functions. *Nat. Chem. Biol.* **2021**, *17* (7), 755−766.

https://doi.org/10.1021/acschembio.4c00633
ACS Chem. Biol. 2024, 19, 2406−2411